Supplementary Information

Mapping the Intrinsic Absorption Properties and Photodegradation Pathways of the Protonated and Deprotonated Forms of the Sunscreen Oxybenzone

Natalie G. K. Wong, Jacob A. Berenbeim, Mathew Hawkridge, Edward Matthews and Caroline E. H. Dessent*

Department of Chemistry, University of York, Heslington, York, YO10 5DD, UK.

* Corresponding author: E-mail caroline.dessent@york.ac.uk

Supplementary Material

S1. Electron Detachment Spectrum of Deprotonated Oxybenzone

S2. Geometries of Deprotonated and Protonated Oxybenzone and Selected Physical Properties

S3. Collision-Induced Dissociation of Deprotonated and Protonated Oxybenzone

S4. Additional Photofragment Action Spectra for Protonated Oxybenzone

S5. Solution-Phase UV Absorption Spectra of Oxybenzone in Variable Methanol-Aqueous Mixtures at Known Acidic, Neutral, and Basic pH

S1. Electron Detachment Spectrum of Deprotonated Oxybenzone

Relative electron detachment was determined according to the following equation:

$$\%\ \text{Electron Detachment} = \left(1 - \frac{\sum \text{Int}_{\text{FRAG}}}{\left(\text{Int}_{\text{OFF}} - \text{Int}_{\text{ON}}\right)}\right) \times 100 \qquad [1]$$

The remaining percent of raw photodepletion signal (Int_{OFF}–Int_{ON}) once the contribution of all photofragments are removed is the electron detachment intensity. Int_{FRAG} is the signal intensity for a unique m/z fragment where all are summed to account for a total (> 50 m/z) photofragment intensity.

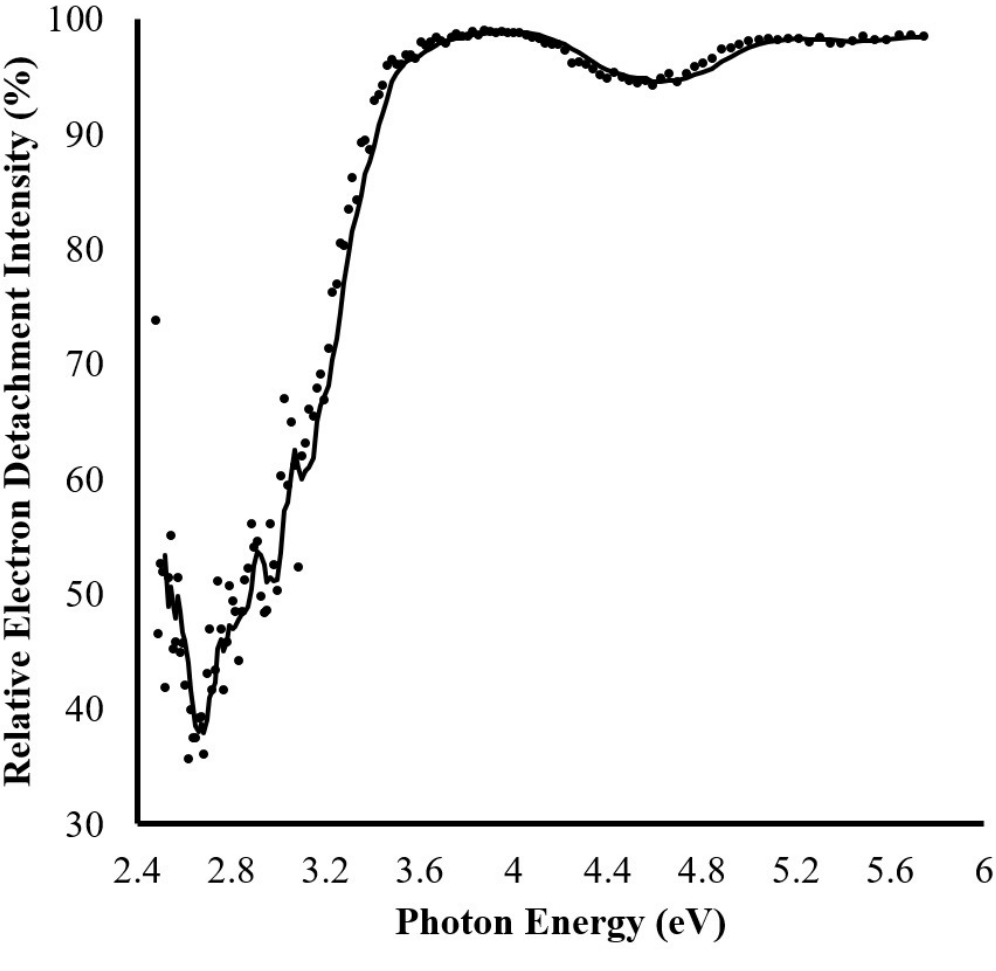

Figure S1. Relative electron detachment intensity of photodissociation of deprotonated oxybenzone ([OB–H]$^-$).

S2. Extensive Geometries of Deprotonated and Protonated Oxybenzone and Selected Physical Properties

Only the lowest energy structures were listed within the manuscript. Here are all inspected structures which include high energy deprotonation site and protomer species. Table S1 includes the energies relative to the lowest energy deprotonated (**D**) or protonated (**P**) structure. Scheme S1 shows the structures found in Table S1.

Table S1. Calculated relative energies and physical properties of OB dependent on pH. Calculated at the ωB97XD/6-311++G** level.

Structure	**Relative Energy (kJ mol^{-1})** [a,b]	**VDE (eV)** [c]	**Vertical Dipole Moment (D)**
D1	0.0 (0.0)	3.00	4.2
D2	8.2 (5.1)	3.00	4.7
D3	21.0 (3.8)	2.89	6.0
D4	29.8 (8.7)	2.87	7.9
D5	159 (150)	2.45	3.4
D6	175 (181)	2.21	5.2
D7	175 (179)	2.17	2.5
D8	191 (158)	2.25	5.9
D9	191 (198)	1.75	5.2
D10	210 (201)	1.94	2.9
P1	0.0 (1.0)		
P2	1.8 (0.0)		
P3	9.9 (9.8)		
P4	16.6 (12.7)		
P5	139 (92)		

Scheme S1. All the structures from Table S1. Arrows indicate the deprotonation site for all **D** structures.

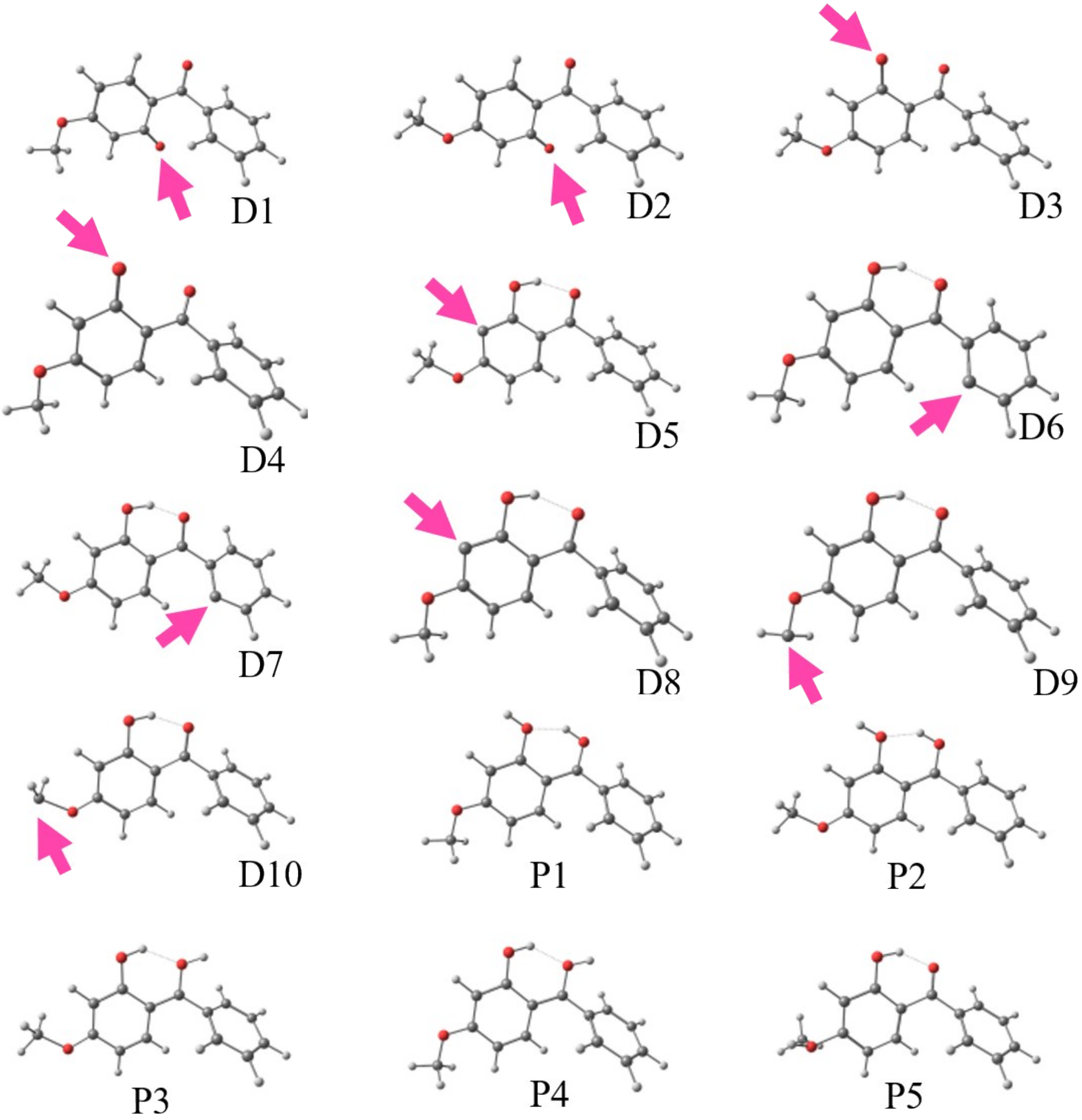

S3. Collision-Induced Dissociation of Deprotonated and Protonated Oxybenzone

Low-energy collision-induced dissociation (CID) was performed on isolated deprotonated and protonated oxybenzone to determine the thermal fragments. Figures S2 and S3 present the relative intensities of the deprotonated and protonated OB parent ion respectively, and the corresponding fragment ions as a function of applied CID energy.

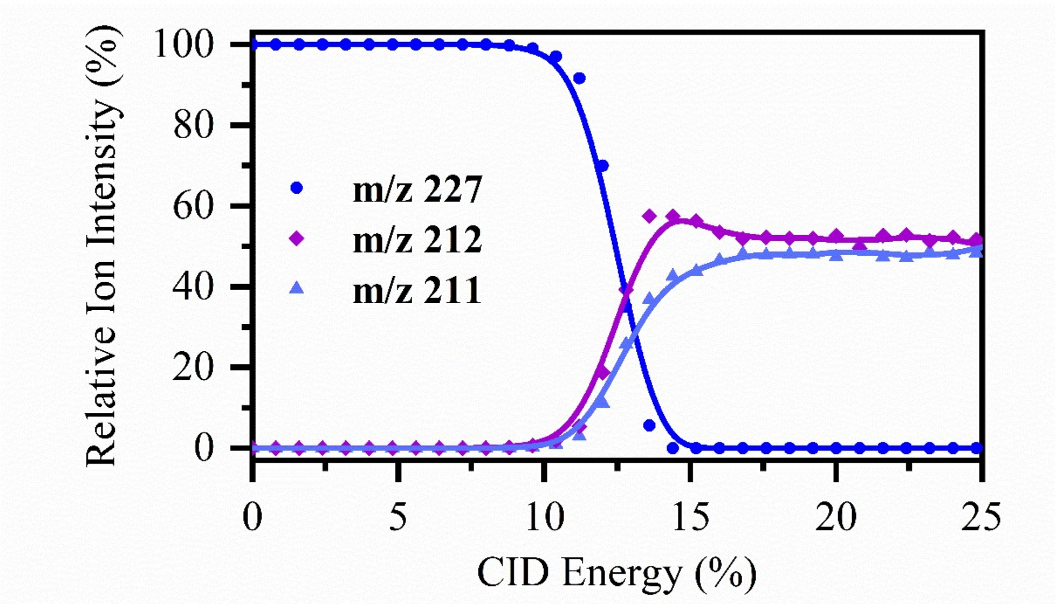

Figure S2. CID fragmentation decay curve for deprotonated oxybenzone (m/z 227) upon low energy CID. Onset plots for production of the associated fragment ions (m/z 212 and m/z 211) are also shown. The curved lines included with the data points are a three-point adjacent average of such data points and are provided as a viewing guide, to emphasize the profile for an individual fragment.

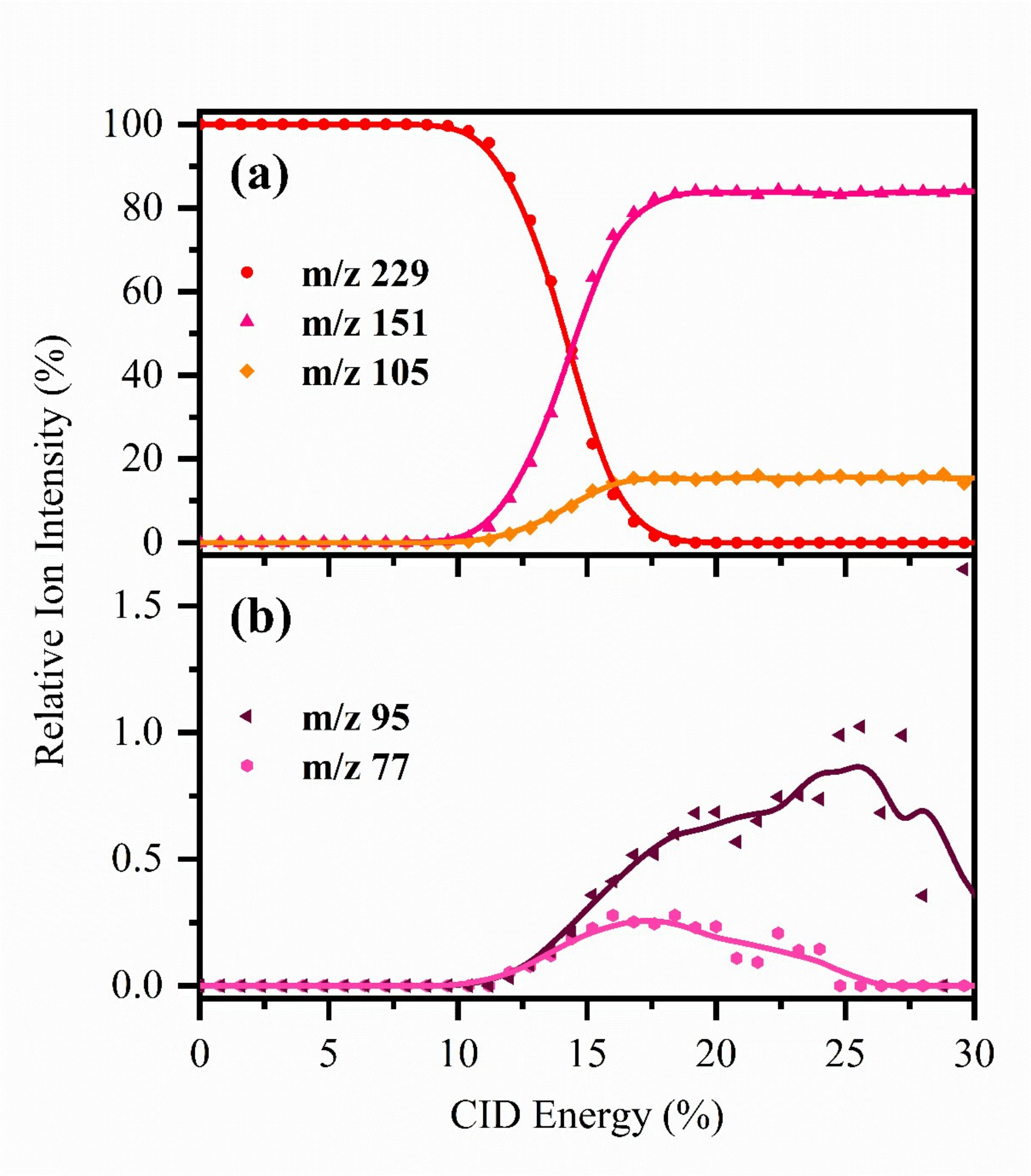

Figure S3. CID fragmentation decay curve for protonated oxybenzone (m/z 229) upon low energy CID. Onset plots for production of the associated fragment ions **(a)** m/z 151 and 105, and **(b)** m/z 95 and 77 are also shown. The curved lines included with the data points are a three-point adjacent average of such data points and are provided as a viewing guide, to emphasize the profile for an individual fragment.

S4. Additional Photofragment Action Spectra for Protonated Oxybenzone

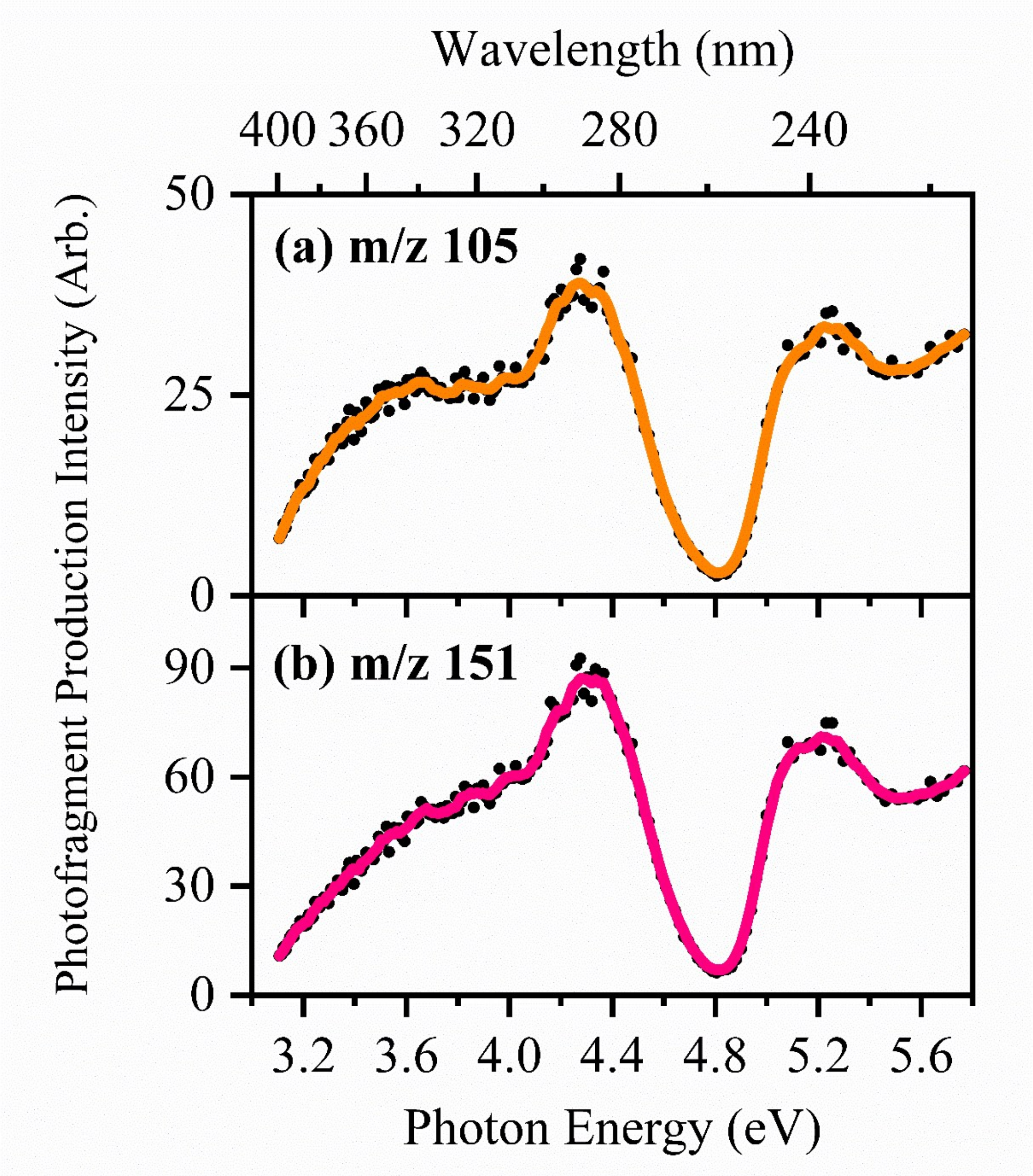

Figure S4. Protonated oxybenzone photofragmentation action spectra of **(a)** m/z 105 and **(b)** m/z 151. The solid line is a five-point adjacent average of the data points.

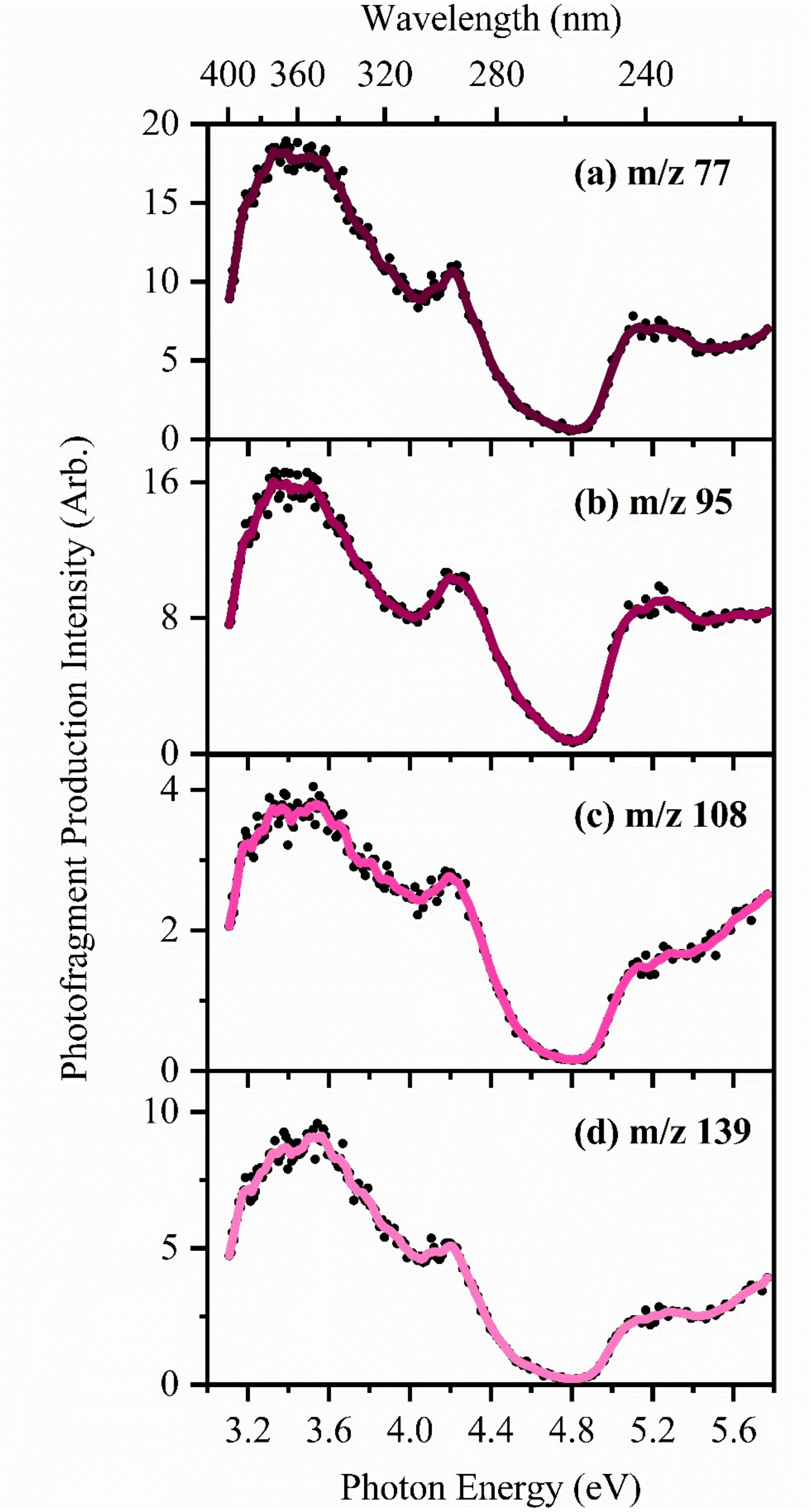

Figure S5. Protonated oxybenzone photofragmentation action spectra of **(a)** m/z 77, **(b)** m/z 95, **(c)** m/z 108, and **(d)** m/z 139. The solid line is a five-point adjacent average of the data points.

S5. Solution-Phase UV Absorption Spectra of Oxybenzone in Variable Methanol-Aqueous Mixtures at Known Acidic, Neutral, and Basic pH

Solution-phase UV absorption spectra of oxybenzone (OB) (1×10^{-5} mol dm^{-3}) in methanol-aqueous mixtures were recorded using a UV-1800 UV-Visible spectrophotometer (Shimadzu, Kyoto, Japan) with a 10 mm UV quartz cuvette. The mass-percent composition of methanol to buffered aqueous solution was varied while the pH and [OB] were held constant. Mixtures were prepared using HPLC-grade MeOH and required the use of NIST standard pH = 7.0 (phosphate) buffer solutions to provide the aqueous component. Here, HCl (3.0 M) and NaOH (2.0 M) were added to pH = 7.0 buffer solutions to achieve the desired protonated and deprotonated forms of OB at pH = 2.95 and 13.0, respectively. Basic mixture solutions > 10% MeOH are not shown due to the precipitation of phosphate buffer under those conditions. OB is poorly soluble in water therefore a 0% MeOH mixture is not shown.

Acidic, neutral, and basic methanol solution conditions shown in Figure S6a-c yield UV spectra are comparable to those methanol-aqueous mixtures of pH = 2.95, 7.0, and 13.0 buffered solutions, respectively. These results are consistent with previously published OB spectra by Li *et al*. (26) and by Baughman *et al*. (50), references found in main article. Issues of miscibility likely account for small shifts of absorbance intensity.

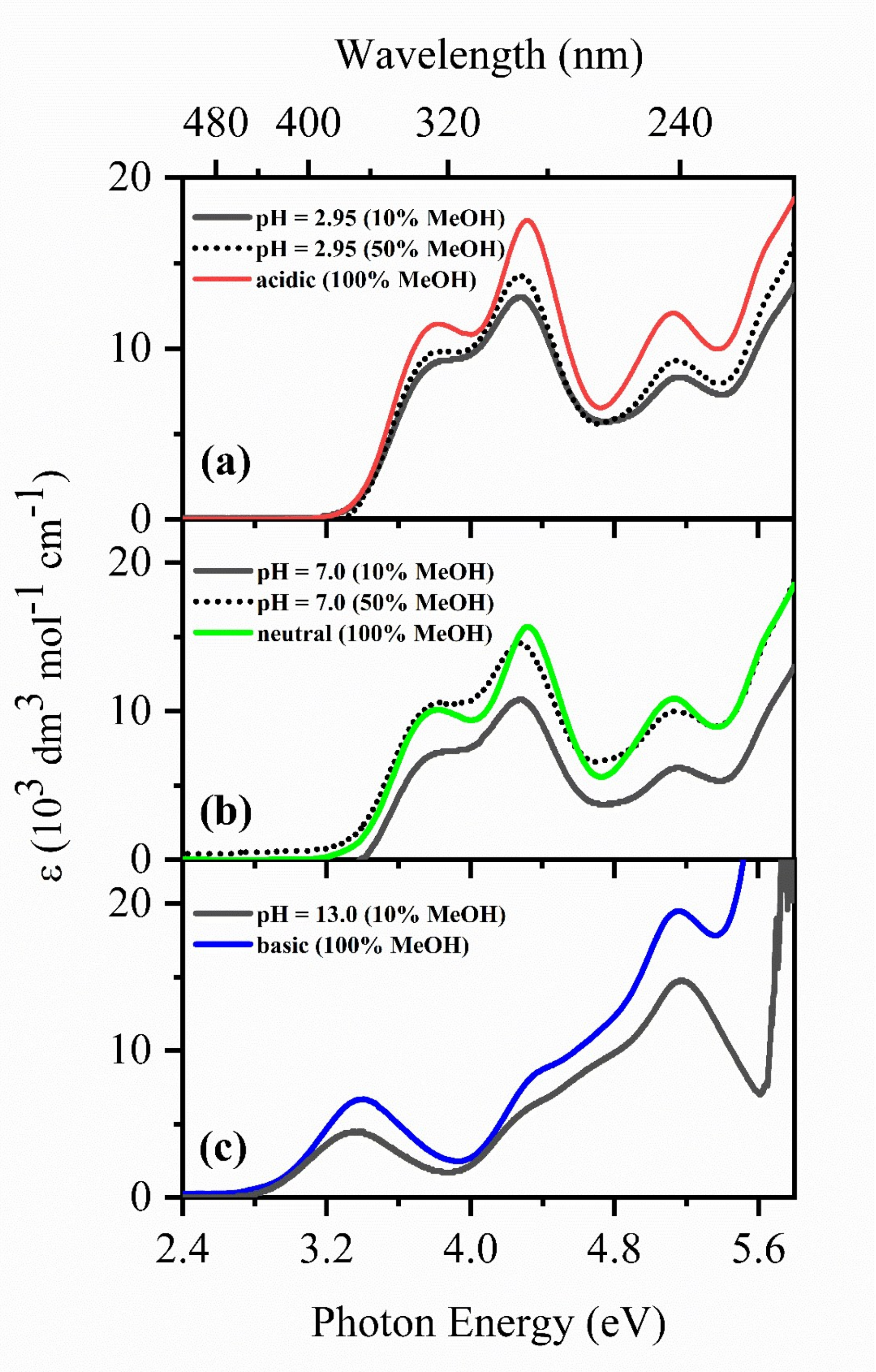

Figure S6. (a) Solution-phase absorption spectrum of OB mixture at pH = 2.95. **(b)** Solution-phase absorption spectra of OB mixture at pH = 7.0. **(c)** Solution-phase absorption spectrum of OB mixture at pH = 13.0.